Effective Slip for Stokes Flow Between Two Grooved Walls with an Arbitrary Phase Shift

Chiu-On Ng[1]

Department of Mechanical Engineering, The University of Hong Kong,
Pokfulam Road, Hong Kong

Abstract

This work aims to determine how the effective slip length for a wall-bounded flow may depend on, among other geometrical parameters, the phase shift between patterns on the two walls. An analytical model is developed for Stokes flow through a channel bounded by walls patterned with a regular array of rectangular ribs and grooves, where the patterns on the two walls can be misaligned by any phase shift. This study incorporates several previous studies as limiting or special cases. It is shown that the phase shift can have qualitatively different effects on the flow rate and effective slip length, depending on the flow direction. In a narrow channel, increasing the phase shift may mildly decrease the flow rate and effective slip length for flow parallel to the grooves, but can dramatically increase the flow rate and effective slip length for flow transverse to the grooves. It is found that unless the channel height is much larger than the period of the wall pattern, the effect due to wall confinement has to be taken into account on evaluating the effective slip lengths.

Keywords: Effective slip length; grooved wall; lubricant infused surface; eigenfunction expansions; wall confinement.

[1]Tel: (852) 2859 2622; Fax: (852) 2858 5415; E-mail address: cong@hku.hk (C.-O. Ng).

1 Introduction

It is a classical problem to determine the slip velocity above a structured surface, which can be an interface between fluid and a medium made up of a composite of fluid and solid. Classical works include, among others, Beavers and Joseph (1967) and Richardson (1971) for a boundary condition at an interface between fluid and a porous material, and also Philip (1972) for flow over a surface of mixed no-slip and no-shear conditions.

The growing demand for flow in ever smaller channels has prompted a renewed interest in studying flow over a micro-textured surface in recent years. The primary interest is to find out how much effective slip or drag reduction can be achieved on replacing a no-slip boundary by a boundary of mixed no-slip and slip conditions. Such micro-textured surfaces can be the so-called superhydrophobic surfaces (e.g. Choi et al. 2003, Ou et al. 2004), slippery liquid-infused porous surfaces (e.g. Wong et al. 2011) or lubricant-impregnated surfaces (e.g. Smith et al. 2013). Studies on these kinds of material surfaces abound in the literature.

One of the micro-structured surfaces that has been extensively studied is a corrugated surface with a regular array of parallel grooves (e.g. Luchini et al. 1991, Wang 2003, Maynes et al. 2007, Teo and Khoo 2009, Ng and Wang 2009, Teo and Khoo 2010, Ng et al. 2010, Mohammadi and Floryan 2013b). In particular, Wang (2003) presented a semi-analytical model, using eigenfunction expansions and matching, for Stokes flow over a surface with parallel rectangular grooves. Considering flow produced by boundary shear, Wang evaluated the effective slip lengths for flow both along and transverse to the grooves. Such effective slip lengths are applicable to a semi-infinite fluid flowing above the surface. Although he also considered flow in a channel with grooved walls, Wang did not look into how channel confinement might affect the slip lengths. When two grooved surfaces are brought in close proximity, the flow between them will be under the combined effects of both surfaces, and the resultant effective slip can be much different from that above a single surface (Cheng et al. 2009, Ng and Chen 2013). When channel wall confinement is considered significant, two parameters will become influential in the problem. One is the distance between the two walls, and another is the phase shift between the patterns on the two walls. The following questions can be asked. How far apart should the two walls be placed so that the effect of

channel wall confinement on the effective slip may or may not be ignored? Also, how far apart should the two walls be separated so that the phase shift will or will not materially affect the effective slip? If the phase shift is influential, in what way will it affect the slip length as a function of the flow direction and other parameters? These questions remain largely unanswered to this date.

To provide answers to these questions, the present work aims to study Stokes flow between two grooved walls, where the flow can be along or transverse to the grooves, and there can be an arbitrary phase shift between the patterns on the two walls. The present problem incorporates several previous studies as limiting or special cases. When the distance between the walls is infinitely large, our problem reduces to that of Wang (2003). In the case of symmetric or staggered longitudinal ribs, our problem reduces to that of Wang (1994). In the case of symmetric or staggered transverse thin fins, our problem then reduces to that of Wang (1997). In Wang (1994, 1997), the focus was on the flow resistance, and the effective slip was not documented in these studies.

The present work models, for the first time, slip flow in a channel bounded by grooved walls, where the grooves on the two walls may be misaligned by any phase shift. As in Wang (1994, 1997, 2003), we shall use the method of domain decomposition and eigenfunction expansions to solve the problem. Because of the arbitrary phase shift, our problem is more complicated in formulation than the previous problems. The problem formulation is described in detail in Section 2, where we introduce the basic solutions in terms of Fourier series for the longitudinal and transverse flows. Low-Reynolds-number flow is considered so that inertia of the flow can be ignored. The domain is decomposed into two regions: one for the clear fluid between the two walls, and one for the fluid in a groove. The Fourier coefficients are determined, on making use of the orthogonality of the eigenfunctions, by matching velocity, stress or pressure on the interface between the two domains, as well as the no-slip conditions on the bottom and side walls of the groove. In Section 3, results are presented to reveal the dependence of the flow and the effective slip length on the flow direction, the phase shift, the channel height, as well as the depth and width of a groove. For some limiting or particular cases, our results can be checked to agree with those available in the literature. We shall show how the phase shift may have qualitatively different effects on the longitudinal and

transverse flow rates and effective slip lengths. We shall also show that the phase effect will have appreciable effect on the slip lengths only when the channel height is not larger than one period of the wall pattern. In sharp contrast, the effect of channel wall confinement on the slip lengths may persist until the channel height is several orders of magnitude larger than the period of the wall pattern.

2 Problem Formulation

We consider pressure-driven flow through a channel bounded by two walls that are each patterned with evenly spaced rectangular ribs and grooves. The applied pressure gradient can be in a direction parallel or normal to the grooves. Figure 1(a) shows a representative cross section of the channel, where the length dimensions have been normalized by half the period of the grooves, L. The normalized period length is therefore 2. Each groove has a normalized width of $2a$, and a normalized depth of b, where $0 \leq a \leq 1$ can be interpreted as the surface area fraction of the wall being occupied by grooves. Each solid rib has a normalized thickness of $2(1-a)$. Note that at the upper limit of $a = 1$, the ribs do not vanish but they reduce to thin fins, as shown in figure 1(c). At the lower limit of $a = 0$, the grooves disappear and the channel will reduce to a slit channel of height $2h$. The two walls are separated by a normalized distance of $2h$ apart, and can be misaligned such that there is a phase shift of $0 \leq \phi \leq 1$ between the two patterns. The two wall patterns are in phase when $\phi = 0$, and half a period out of phase when $\phi = 1$, corresponding to the symmetric and staggered configurations, respectively.

For convenience of analysis, two Cartesian coordinate systems are introduced as shown in figure 1. The origin of (x, y) is placed at a point on the centerline of channel that is halfway between the centerlines of Ribs 2 and 3. The origin of (x', y') is located at a point on the envelope of the lower wall that is halfway between the centerlines of Ribs 1 and 3. We shall use the coordinates (x, y) for the layer of clear fluid between the two walls $-h \leq y \leq h$, called Region I. The coordinates (x', y') are used for the fluid in the groove between Ribs 1 and 3 $(-a \leq x' \leq a, -b \leq y' \leq 0)$, called Region II. In other words, Region I is the clear fluid layer of height $2h$, while Region II is the cavity between two ribs; see figure 1(b). The envelope of

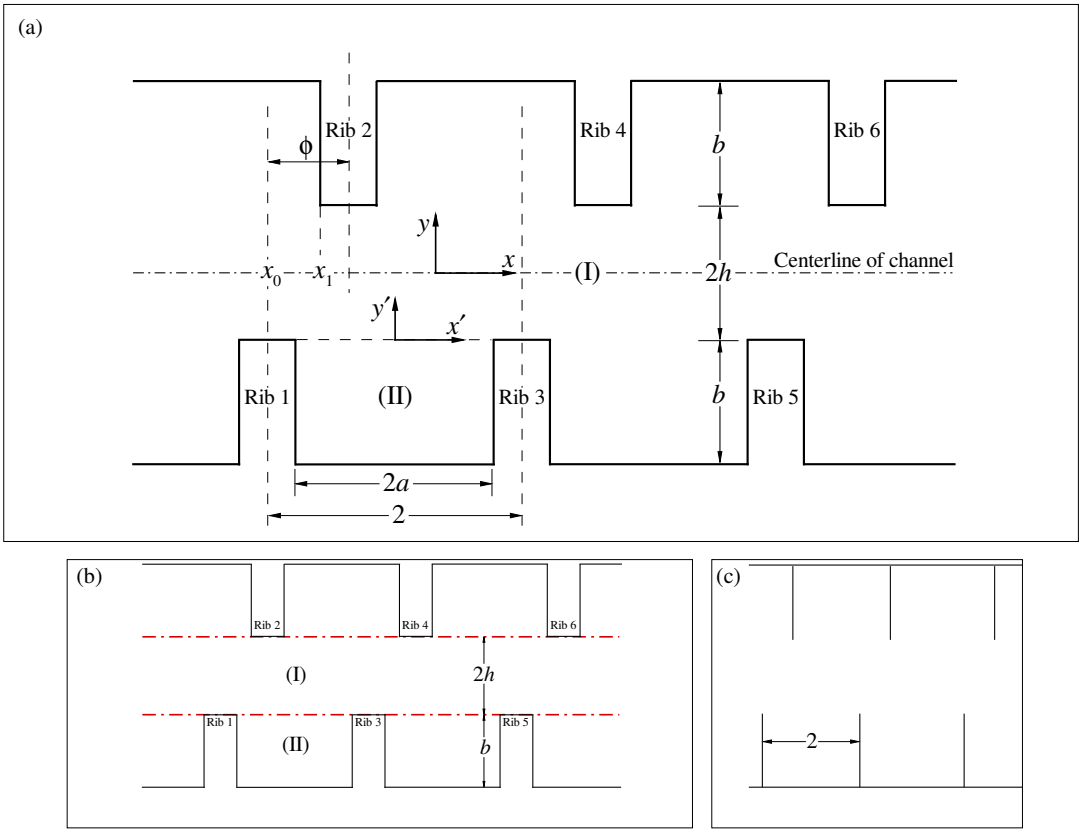

Figure 1: (a) Cross section of a channel bounded by two structured walls with a regular array of rectangular grooves of width $2a$ and depth b, where the lengths are normalized by half the period of the grooves. The two walls are separated by a clear distance of $2h$ apart, and opposite ribs can be misaligned by a phase shift ϕ. Coordinates (x, y) are for flow in Region I, and coordinates (x', y') are for flow in Region II. As shown in (b), Region I is the clear fluid layer between the two grooved walls, and Region II is the groove between Ribs 1 and 3. The interface between Regions I and II is the envelope of the lower grooved wall. The limiting case of $a = 1$, or ribs reducing to thin fins, is shown in (c).

the lower grooved wall is the interface between Regions I and II. The two coordinate systems are related to each other by

$$x' = x + \phi/2, \quad y' = y + h. \tag{1}$$

2.1 Longitudinal flow

We first consider flow driven by a pressure gradient $K_z \equiv -\mathrm{d}p/\mathrm{d}z$ that is directed parallel to the grooves, and the resultant flow is in the z-direction (i.e. normal to the x-y plane). The governing equation is

$$\frac{\partial^2 w}{\partial x^2} + \frac{\partial^2 w}{\partial y^2} = -1, \tag{2}$$

where w is the velocity normalized by $K_z L^2/\mu$, in which μ is the fluid viscosity.

In Region I, the flow has polar symmetry, i.e. $w_{\mathrm{I}}(x,y) = w_{\mathrm{I}}(-x,-y)$ and $w_{\mathrm{I}}(x,-y) = w_{\mathrm{I}}(-x,y)$. The general solution for Region I that satisfies such symmetry and periodicity in the x-direction can be written as

$$\begin{aligned} w_{\mathrm{I}}(x,y) &= \frac{1}{2}\left(h^2 - y^2\right) + A_0 + \sum_{n=1}^{\infty} A_n \cos(\alpha_n x)\frac{\cosh(\alpha_n y)}{\cosh(\alpha_n h)} \\ &\quad + \sum_{n=1}^{\infty} B_n \sin(\alpha_n x)\frac{\sinh(\alpha_n y)}{\sinh(\alpha_n h)}, \end{aligned} \tag{3}$$

where A_0, A_n and B_n are undetermined coefficients, and $\alpha_n = n\pi$. In the above solution, the first term is the particular solution, corresponding to the classical parabolic velocity profile for Poiseuille flow through a no-slip parallel-plate channel. The constant A_0 is to account for the effective slip arising from the grooved walls. The two infinite series are eigenfunction expansions to describe how the flow will change as a periodic function of x with a period of $2/n$, for $n = 1, 2, \cdots$.

The general solution for Region II that satisfies no-slip at $y' = -b$ is

$$\begin{aligned} w_{\mathrm{II}}(x',y') &= -\frac{1}{2}\left(y'^2 + by'\right) + \sum_{n=1}^{\infty} C_n \cos(\beta_n x')\left[e^{\beta_n y'} - e^{-\beta_n(y'+2b)}\right] \\ &\quad + \sum_{n=1}^{\infty} D_n \sin(\gamma_n x')\left[e^{\gamma_n y'} - e^{-\gamma_n(y'+2b)}\right] + \sum_{n=1}^{\infty} E_n \frac{\cosh(\sigma_n x')}{\cosh(\sigma_n a)}\sin(\sigma_n y'), \end{aligned} \tag{4}$$

where C_n, D_n and E_n are undetermined coefficients, $\beta_n = (n - 1/2)\pi/a$, $\gamma_n = n\pi/a$, and $\sigma_n = n\pi/b$. Here, the first term is the particular solution satisfying no-slip at the bottom.

The other terms are eigenfunction expansions in the form of Fourier series satisfying no-slip at the lateral and/or the bottom boundaries.

Let us truncate the series to finite terms: A_n and B_n each to M terms, C_n and D_n each to N terms, and E_n to P terms, such that $N \approx \text{Integer}[aM]$ and $P \approx \text{Integer}[bM]$. These coefficients are to be determined using the following matching and boundary conditions.

The no-slip condition on the two side walls of the groove requires $w_{\text{II}}(x' = \pm a) = 0$, which amounts to

$$\sum_{n=1}^{P} E_n \sin(\sigma_n y') = \frac{1}{2}\left(y'^2 + by'\right). \tag{5}$$

Multiplying this equation by $\sin(\sigma_m y')$ and integrating with respect to y' from $-b$ to 0 gives

$$E_m = \frac{2\left[1 + (-1)^{m+1}\right]}{\sigma_m^3 b}, \qquad m = 1, \cdots, P. \tag{6}$$

The matching conditions for the continuity of velocity and shear stress on $y = -h$ or $y' = 0$ are

$$w_{\text{I}} = \begin{cases} w_{\text{II}} & \text{for } -a < x' < a \\ 0 & \text{for } -1 \le x' < -a,\ a < x' \le 1 \end{cases}, \tag{7}$$

and

$$\frac{\partial w_{\text{I}}}{\partial y} = \frac{\partial w_{\text{II}}}{\partial y'} \quad \text{for } -a < x' < a. \tag{8}$$

Integrating equation (7) with respect to x from $-1 - \phi/2$ to $1 - \phi/2$ (or with respect to x' from -1 to 1) gives

$$A_0 = \sum_{n=1}^{N} \frac{(-1)^{n+1}}{\beta_n}\left(1 - e^{-2\beta_n b}\right) C_n. \tag{9}$$

On multiplying equation (7) by $\cos(\alpha_m x)$, followed by integration with respect to x from $-1 - \phi/2$ to $1 - \phi/2$, we get

$$A_m - \sum_{n=1}^{N} I_{mn}^{(1)}\left(1 - e^{-2\beta_n b}\right) C_n - \sum_{n=1}^{N} I_{mn}^{(2)}\left(1 - e^{-2\gamma_n b}\right) D_n = 0, \qquad m = 1, \cdots, M, \tag{10}$$

where

$$I_{mn}^{(1)} = \cos(\alpha_m \phi/2) \times \begin{cases} \left(\frac{\sin[(\alpha_m - \beta_n)a]}{\alpha_m - \beta_n} + \frac{\sin[(\alpha_m + \beta_n)a]}{\alpha_m + \beta_n}\right) & \text{for } \alpha_m \ne \beta_n \\ a & \text{for } \alpha_m = \beta_n \end{cases}, \tag{11}$$

$$I_{mn}^{(2)} = \sin(\alpha_m \phi/2) \times \begin{cases} \left(\frac{\sin[(\alpha_m - \gamma_n)a]}{\alpha_m - \gamma_n} - \frac{\sin[(\alpha_m + \gamma_n)a]}{\alpha_m + \gamma_n}\right) & \text{for } \alpha_m \ne \gamma_n \\ a & \text{for } \alpha_m = \gamma_n \end{cases}. \tag{12}$$

On multiplying equation (7) by $\sin(\alpha_m x)$, followed by integration with respect to x from $-1-\phi/2$ to $1-\phi/2$, we get

$$B_m + \sum_{n=1}^{N} I_{mn}^{(3)} \left(1 - e^{-2\beta_n b}\right) C_n + \sum_{n=1}^{N} I_{mn}^{(4)} \left(1 - e^{-2\gamma_n b}\right) D_n = 0, \qquad m = 1, \cdots, M, \tag{13}$$

where

$$I_{mn}^{(3)} = -\sin(\alpha_m \phi/2) \times \begin{cases} \left(\frac{\sin[(\alpha_m - \beta_n)a]}{\alpha_m - \beta_n} + \frac{\sin[(\alpha_m + \beta_n)a]}{\alpha_m + \beta_n}\right) & \text{for } \alpha_m \neq \beta_n \\ a & \text{for } \alpha_m = \beta_n \end{cases}, \tag{14}$$

$$I_{mn}^{(4)} = \cos(\alpha_m \phi/2) \times \begin{cases} \left(\frac{\sin[(\alpha_m - \gamma_n)a]}{\alpha_m - \gamma_n} - \frac{\sin[(\alpha_m + \gamma_n)a]}{\alpha_m + \gamma_n}\right) & \text{for } \alpha_m \neq \gamma_n \\ a & \text{for } \alpha_m = \gamma_n \end{cases}. \tag{15}$$

On multiplying equation (8) by $\cos(\beta_m x')$, followed by integration with respect to x' from $-a$ to a, we get after substituting equation (6) for E_m

$$\begin{aligned} &\sum_{n=1}^{M} I_{nm}^{(1)} \alpha_n \tanh(\alpha_n h) A_n - \sum_{n=1}^{M} I_{nm}^{(3)} \alpha_n \coth(\alpha_n h) B_n + \beta_m a \left(1 + e^{-2\beta_m b}\right) C_m \\ &\quad = 2\left(h + \frac{b}{2}\right) \frac{\sin(\beta_m a)}{\beta_m} - \sum_{n=1}^{P} \frac{(-1)^{m+1} 4 \left[1 + (-1)^{n+1}\right] \beta_m}{\sigma_n^2 b \left(\beta_m^2 + \sigma_n^2\right)}, \qquad m = 1, \cdots, N, \end{aligned} \tag{16}$$

On multiplying equation (8) by $\sin(\gamma_m x')$, followed by integration with respect to x' from $-a$ to a, we get

$$\begin{aligned} &\sum_{n=1}^{M} I_{nm}^{(2)} \alpha_n \tanh(\alpha_n h) A_n - \sum_{n=1}^{M} I_{nm}^{(4)} \alpha_n \coth(\alpha_n h) B_n \\ &\qquad + \gamma_m a \left(1 + e^{-2\gamma_m b}\right) D_m = 0, \qquad m = 1, \cdots, N. \end{aligned} \tag{17}$$

Equations (10), (13), (16) and (17) constitute a system of $2(M+N)$ equations that can be solved for the same number of unknown coefficients: $A_{1,\cdots,M}$, $B_{1,\cdots,M}$, $C_{1,\cdots,N}$ and $D_{1,\cdots,N}$. In this work, we have chosen to use the routine IMSL-DLSARG to solve the system of equations.

The rate of volume flow per unit width of the channel is given by the sum of those in Regions I and II:

$$q_{\parallel} = q_{\mathrm{I}\parallel} + 2q_{\mathrm{II}\parallel}, \tag{18}$$

where the factor of 2 is to account for grooves on the upper and lower walls, and

$$q_{\mathrm{I}\parallel} = \frac{1}{2} \int_{-h}^{h} \int_{-1}^{1} w_{\mathrm{I}} \mathrm{d}x \mathrm{d}y = \frac{2h^3}{3} + 2hA_0, \tag{19}$$

$$q_{\text{II}\parallel} = \frac{1}{2}\int_{-b}^{0}\int_{-a}^{a} w_{\text{II}}\mathrm{d}x'\mathrm{d}y'$$
$$= \frac{ab^3}{6} + 2\sum_{n=1}^{N}(-1)^{n+1}\frac{C_n}{\beta_n^2}\left(1-e^{-\beta_n b}\right)^2 - 4\sum_{n=1}^{P}\frac{\tanh(\sigma_n a)}{\sigma_n^5 b}\left[1+(-1)^{n+1}\right]^2. \quad (20)$$

If we consider that the flow in the grooves (Region II) serves to lubricate the flow in the clear fluid layer (Region I), we may compare $q_{\text{I}\parallel}$ to $q = 2h^3/3 + 2\lambda h^2$, which is the flow rate through a channel of height of $2h$ bounded by walls of equal slip length λ (see Appendix I). Thereby, the effective slip length for the longitudinal flow can be evaluated as follows:

$$\lambda_\parallel = \frac{q_{\text{I}\parallel} - 2h^3/3}{2h^2} = \frac{A_0}{h}. \quad (21)$$

Note that the effective slip length defined above is the boundary slip length of an equivalent uniform channel of height $2h$ such that, under the same pressure forcing, the flow rate through the equivalent channel is the same as that through a clear fluid layer of height $2h$ bounded by walls with longitudinal grooves. The effective slip length defined this way is always non-negative, simply because the baseline for this slip length is the envelope of the grooved wall. The flow below this baseline can only lubricate the flow above it. Also note that the flow rate below this baseline, $q_{\text{II}\parallel}$, is excluded in the definition above. A positive effective slip length here means an enhanced flow rate when compared with that through a uniform channel of height $2h$ bounded by no-slip walls.

For illustration, we show in table 1 how the computed value of $\lambda_\parallel$ may converge as the number of terms M increases. Typically, a four-digit accuracy can be attained when M is about 50, which is consistent with that reported by Wang (2003).

Table 1: Convergence of $\lambda_\parallel$ when $a = 0.9$, $h = 1$, $\phi = 0$.

M	20	50	100	150
$b = 0.1$	0.08216	0.08223	0.08224	0.08224
$b = 1$	0.4191	0.4193	0.4193	0.4193

2.2 Transverse flow

We next consider Stokes flow driven by a pressure gradient $K_x \equiv -\mathrm{d}p_0/\mathrm{d}x$ that is normal to the grooves, where p_0 is the externally applied pressure. The resultant flow is two dimensional as a function of x and y, with the x-direction being the principal direction of flow. The governing equations are

$$\frac{\partial u}{\partial x} + \frac{\partial v}{\partial y} = 0, \tag{22}$$

$$\frac{\partial^2 u}{\partial x^2} + \frac{\partial^2 u}{\partial y^2} = -1 + \frac{\partial p}{\partial x}, \tag{23}$$

$$\frac{\partial^2 v}{\partial x^2} + \frac{\partial^2 v}{\partial y^2} = \frac{\partial p}{\partial y}, \tag{24}$$

where (u, v) are the x- and y-components of velocity normalized by $K_x L^2/\mu$, and p is the internally induced pressure.

For Region I, the general solutions for the velocity components that satisfy polar symmetry and periodicity in the x-direction are as follows:

$$\begin{aligned} u_{\mathrm{I}}(x,y) &= \frac{1}{2}\left(h^2 - y^2\right) + A_0 + \sum_{n=1}^{\infty} \frac{\cos(\alpha_n x)}{\cosh(\alpha_n h)} \left[(A_n + B_n)\cosh(\alpha_n y) + B_n \alpha_n y \sinh(\alpha_n y)\right] \\ &\quad - \sum_{n=1}^{\infty} \frac{\sin(\alpha_n x)}{\cosh(\alpha_n h)} \left[(C_n + D_n)\sinh(\alpha_n y) + D_n \alpha_n y \cosh(\alpha_n y)\right], \end{aligned} \tag{25}$$

$$\begin{aligned} v_{\mathrm{I}}(x,y) &= \sum_{n=1}^{\infty} \frac{\sin(\alpha_n x)}{\cosh(\alpha_n h)} \left[A_n \sinh(\alpha_n y) + B_n \alpha_n y \cosh(\alpha_n y)\right] \\ &\quad + \sum_{n=1}^{\infty} \frac{\cos(\alpha_n x)}{\cosh(\alpha_n h)} \left[C_n \cosh(\alpha_n y) + D_n \alpha_n y \sinh(\alpha_n y)\right], \end{aligned} \tag{26}$$

where A_0, A_n, B_n, C_n, D_n are coefficients to be determined, and $\alpha_n = n\pi$. The first term in equation (25) is the particular solution, corresponding to the classical parabolic velocity profile for Poiseuille flow through a no-slip slit channel. The constant A_0 is to account for the effective slip arising from the grooved walls. The other terms are eigenfunction expansions to describe the periodicity of the solution in the x-direction.

For Region II, the general solutions for the velocity components can be expressed in terms of eigenfunction expansions as follows:

$$u_{\mathrm{II}}(x', y') = \sum_{n=1}^{\infty} \cos(\beta_n x') U_{1n}(y') + \sum_{n=1}^{\infty} \sin(\gamma_n x') U_{2n}(y') + \sum_{n=1}^{\infty} \cos(\sigma_n y') U_{3n}(x'), \tag{27}$$

$$v_{\rm II}(x',y') = \sum_{n=1}^{\infty} \sin(\beta_n x') V_{1n}(y') + \sum_{n=1}^{\infty} \cos(\gamma_n x') V_{2n}(y') + \sum_{n=1}^{\infty} \sin(\sigma_n y') V_{3n}(x'), \qquad (28)$$

where $\beta_n = (n-1/2)\pi/a$, $\gamma_n = n\pi/a$, $\sigma_n = n\pi/b$. To satisfy $u_{\rm II}(x' = \pm a) = 0$ and $v_{\rm II}(y' = -b) = 0$, we may deduce that

$$\begin{aligned} U_{1n}(y') &= E_n \left[e^{\beta_n y'} + e^{-\beta_n (y'+2b)} \right] + F_n \left[1 + \beta_n (y'+b) \right] e^{\beta_n y'} \\ &\quad + G_n \left[1 - \beta_n (y'+b) \right] e^{-\beta_n (y'+b)}, \end{aligned} \qquad (29)$$

$$\begin{aligned} V_{1n}(y') &= E_n \left[e^{\beta_n y'} - e^{-\beta_n (y'+2b)} \right] + F_n \beta_n (y'+b) e^{\beta_n y'} \\ &\quad + G_n \beta_n (y'+b) e^{-\beta_n (y'+b)}, \end{aligned} \qquad (30)$$

$$\begin{aligned} U_{2n}(y') &= H_n \left[e^{\gamma_n y'} + e^{-\gamma_n (y'+2b)} \right] + K_n \left[1 + \gamma_n (y'+b) \right] e^{\gamma_n y'} \\ &\quad + L_n \left[1 - \gamma_n (y'+b) \right] e^{-\gamma_n (y'+b)}, \end{aligned} \qquad (31)$$

$$\begin{aligned} V_{2n}(y') &= -H_n \left[e^{\gamma_n y'} - e^{-\gamma_n (y'+2b)} \right] - K_n \gamma_n (y'+b) e^{\gamma_n y'} \\ &\quad - L_n \gamma_n (y'+b) e^{-\gamma_n (y'+b)}, \end{aligned} \qquad (32)$$

$$\begin{aligned} U_{3n}(x') &= Q_n \left[\frac{\cosh(\sigma_n x')}{\cosh(\sigma_n a)} - \frac{x' \sinh(\sigma_n x')}{a \sinh(\sigma_n a)} \right] \\ &\quad + R_n \left[\frac{\sinh(\sigma_n x')}{\sinh(\sigma_n a)} - \frac{x' \cosh(\sigma_n x')}{a \cosh(\sigma_n a)} \right], \end{aligned} \qquad (33)$$

$$\begin{aligned} V_{3n}(x') &= Q_n \left[-\frac{\sinh(\sigma_n x')}{\cosh(\sigma_n a)} + \frac{\sinh(\sigma_n x')}{\sigma_n a \sinh(\sigma_n a)} + \frac{x' \cosh(\sigma_n x')}{a \sinh(\sigma_n a)} \right] \\ &\quad + R_n \left[-\frac{\cosh(\sigma_n x')}{\sinh(\sigma_n a)} + \frac{\cosh(\sigma_n x')}{\sigma_n a \cosh(\sigma_n a)} + \frac{x' \sinh(\sigma_n x')}{a \cosh(\sigma_n a)} \right], \end{aligned} \qquad (34)$$

where E_n, F_n, G_n, H_n, K_n, L_n, Q_n, R_n are coefficients to be determined.

Let us truncate the infinite series to finite terms: $A_n, \cdots, D_n$ each to M terms, $E_n, \cdots, L_n$ each to N terms, and Q_n and R_n each to P terms, such that $N \approx$ Integer$[aM]$ and $P \approx$ Integer$[bM]$. These coefficients are to be determined using the following matching and boundary conditions.

The matching conditions for the continuity of velocity, shear stress and pressure on $y = -h$ or $y' = 0$ are as follows:

$$u_{\rm I} = \begin{cases} u_{\rm II} & \text{for } -a < x' < a \\ 0 & \text{for } -1 \le x' < -a,\ a < x' \le 1 \end{cases}, \tag{35}$$

$$v_{\rm I} = \begin{cases} v_{\rm II} & \text{for } -a < x' < a \\ 0 & \text{for } -1 \le x' < -a,\ a < x' \le 1 \end{cases}, \tag{36}$$

$$\frac{\partial u_{\rm I}}{\partial y} = \frac{\partial u_{\rm II}}{\partial y'} \quad \text{for } -a < x' < a, \tag{37}$$

$$\frac{\partial^2 u_{\rm I}}{\partial y^2} = \frac{\partial^2 u_{\rm II}}{\partial y'^2} \quad \text{for } -a < x' < a. \tag{38}$$

The no-slip conditions on the bottom and side walls of the groove further require

$$u_{\rm II} = 0 \qquad \text{for } -a < x' < a,\ y' = -b, \tag{39}$$

$$v_{\rm II} = 0 \qquad \text{for } x' = \pm a,\ -b < y' < 0. \tag{40}$$

Equations for the coefficients can be derived from these matching and boundary conditions, using the orthogonality of the eigenfunctions as in the case of longitudinal flow. The derivation and the equations are provided in Appendix II.

The rate of volume flow per unit spanwise width of the channel is given by

$$q_\perp = \begin{cases} \int_{-h}^{h} u_{\rm I}|_{x=x_0} {\rm d}y & \text{if } \phi \le 1 - a \\ \int_{-h}^{h} u_{\rm I}|_{x=x_0} {\rm d}y - \int_{x_0}^{x_1} v_{\rm I}|_{y=h} {\rm d}x & \text{if } \phi > 1 - a \end{cases}, \tag{41}$$

where $x_0 = -1 - \phi/2$, $x_1 = \phi/2 + a - 2$ (see figure 1), and

$$\int_{-h}^{h} u_{\rm I}|_{x=x_0} {\rm d}y = \frac{2h^3}{3} + 2hA_0 + 2\sum_{n=1}^{M} \frac{\cos(\alpha_n x_0)}{\alpha_n} \left[\tanh(\alpha_n h) A_n + \alpha_n h B_n\right], \tag{42}$$

$$\begin{aligned} -\int_{x_0}^{x_1} v_{\rm I}|_{y=h} {\rm d}x \;\; &= \;\; \sum_{n=1}^{M} \frac{\cos(\alpha_n x_1) - \cos(\alpha_n x_0)}{\alpha_n} \left[\tanh(\alpha_n h) A_n + \alpha_n h B_n\right] \\ &\quad - \sum_{n=1}^{M} \frac{\sin(\alpha_n x_1) - \sin(\alpha_n x_0)}{\alpha_n} \left[C_n + \alpha_n h \tanh(\alpha_n h) D_n\right]. \end{aligned} \tag{43}$$

Again, if we compare this flow rate to $q = 2h^3/3 + 2\lambda h^2$, which is the flow rate through a channel of height $2h$ bounded by walls of constant slip length λ (see Appendix I), we may evaluate the effective slip length for the transverse flow as follows:

$$\lambda_\perp = \frac{q_\perp - 2h^3/3}{2h^2}. \tag{44}$$

Again, this effective slip length corresponds to the boundary slip length of an equivalent uniform channel of height $2h$ such that, under the same pressure gradient, the rate of flow through the equivalent uniform channel is the same as that through a clear fluid layer of height $2h$ bounded by walls with transverse grooves. As the baseline is the envelope of the grooved wall, this effective slip length is non-negative. A positive effective slip length means flow enhancement when compared with the flow through a channel of height $2h$ bounded by no-slip walls.

We show in table 2 some computed values of $\lambda_\perp$ to illustrate the convergence of the solution as M is increased. To attain a three-digit accuracy, $M \approx 200$ is usually sufficient.

Table 2: Convergence of $\lambda_\perp$ when $a = 0.9$, $h = 1$, $\phi = 0$.

M	50	100	150	200	250	300
$b = 0.1$	0.07403	0.07382	0.07375	0.07371	0.07368	0.07366
$b = 1$	0.1648	0.1638	0.1635	0.1634	0.1633	0.1633

3 Results and Discussion

We first examine how the flow rate q is differently affected by the pattern phase shift ϕ, depending on the flow direction. Figure 2 shows $q_\parallel$ and $q_\perp$ as functions of ϕ for various values of a and h. The following observations can be made. For the same wall pattern, the longitudinal flow rate is maximum at $\phi = 0$ (i.e. when the patterns are symmetric), and is minimum at $\phi = 1$ (i.e. when the patterns are staggered). The opposite is true for the transverse flow rate: maximum at $\phi = 1$, and minimum at $\phi = 0$. These trends are

consistent with the findings previously reported by Wang (1976, 1979) for flow between two corrugated plates, and by Ng and Zhou (2012) for electroosmotic flow through a thin channel with gradually varying slip lengths on the two walls. Similar observations have also been made by Mohammadi and Floryan (2012, 2013b, 2013a, 2015) who studied drag reduction in grooved or corrugated channels. We further note that the phase shift will have larger effect on the flow rate for thicker ribs in the case of longitudinal flow, but for thinner ribs in the case of transverse flow; see figures 2(a, b). It is interesting to find that, for thin fins ($a = 1$) in a very narrow channel ($h = 0.05$), variation of ϕ from 0 to 1 can only modestly change $q_{\parallel}$ by a few percent, but will significantly change $q_{\perp}$ by a factor of several times. This is because, in the limit of thin fins, the phase shift has little effect on the longitudinal flow resistance. Transverse flow resistance, on the contrary, can be a strong function of the phase shift, especially in a narrow channel; see further discussion below and figure 4. For transverse thin fins, the flow rate changes with the phase shift largely within the range $0 < \phi < 0.4$; the change is much milder for $0.4 < \phi < 1$. It is also important to note that, for any wall pattern and flow direction, the effect of the phase shift on the flow will diminish as the distance between the two walls increases. Figures 2(e, f) reveal that when $h = O(1)$, the flow rate, for either flow direction, is virtually unaffected by the phase shift.

For the same values of the parameters a, b, h, ϕ, the longitudinal flow rate is always larger than the transverse flow rate, $q_{\parallel} > q_{\perp}$. This concurs with the well-known fact that, for a two-dimensional wall pattern, the flow resistance is always smaller parallel to the pattern than that normal to the pattern. In figures 2(a, c, e), we also show the agreement between our results with those (symbols) computed by Wang (1994), who considered Stokes flow in a channel with longitudinal ribs in a symmetric or staggered configuration.

To illustrate how the flow is affected by the phase shift, we show in figures 3 and 4 the longitudinal and transverse flow fields for $\phi = 0, 0.5, 1$, where $a = 0.9$, and $b = h = 0.5$. Constant velocity lines are shown in figure 3, while streamlines are shown in figure 4. The stream function is found by integrating u with respect to y' or y, where the stream function is set to be zero on the lower wall. When the wall patterns are in phase, $\phi = 0$, the grooves and ribs on one wall are aligned exactly with those on the other wall. Whether or not the grooves/ribs are aligned will have different effects on the longitudinal and transverse flows.

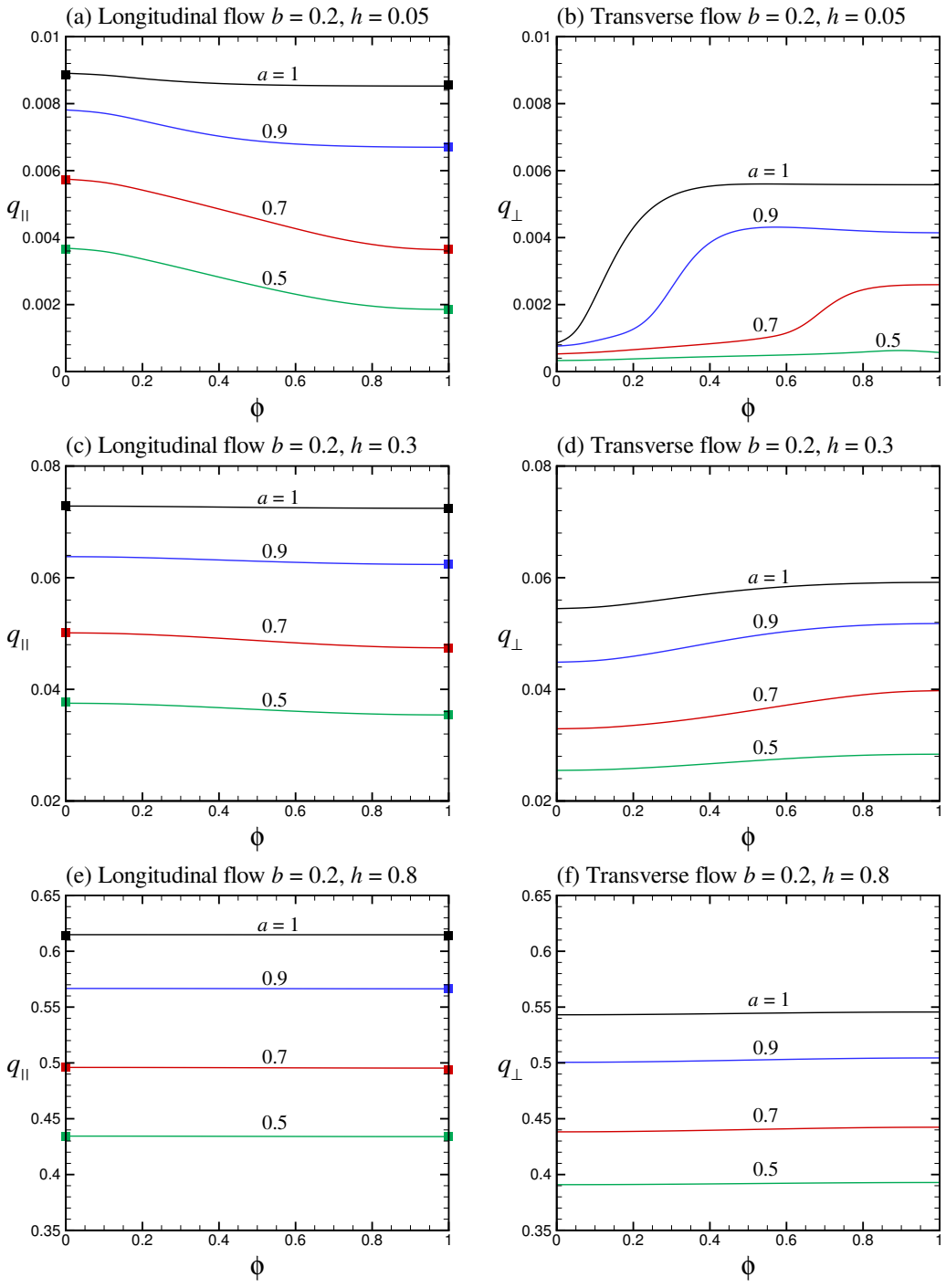

Figure 2: Longitudinal and transverse flow rates, $q_{\|}$ and $q_{\perp}$, as functions of the phase shift ϕ, for various values of a, where $b = 0.2$, and $h = 0.05$, 0.3, 0.8. The symbols are from Wang (1994).

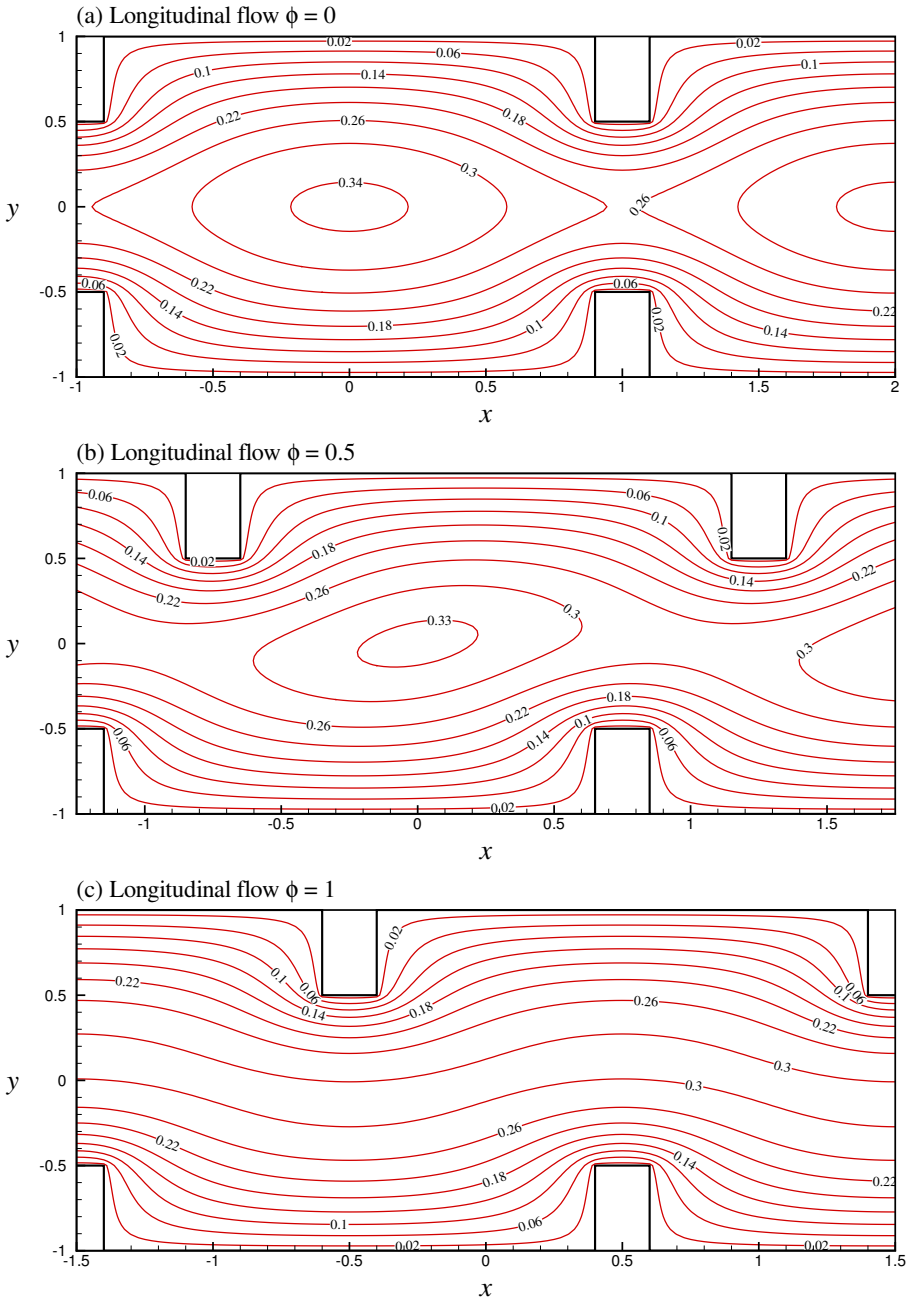

Figure 3: Constant velocity lines for longitudinal flow, with phase shift (a) $\phi = 0$, (b) $\phi = 0.5$, (c) $\phi = 1$, where $a = 0.9$, and $b = h = 0.5$.

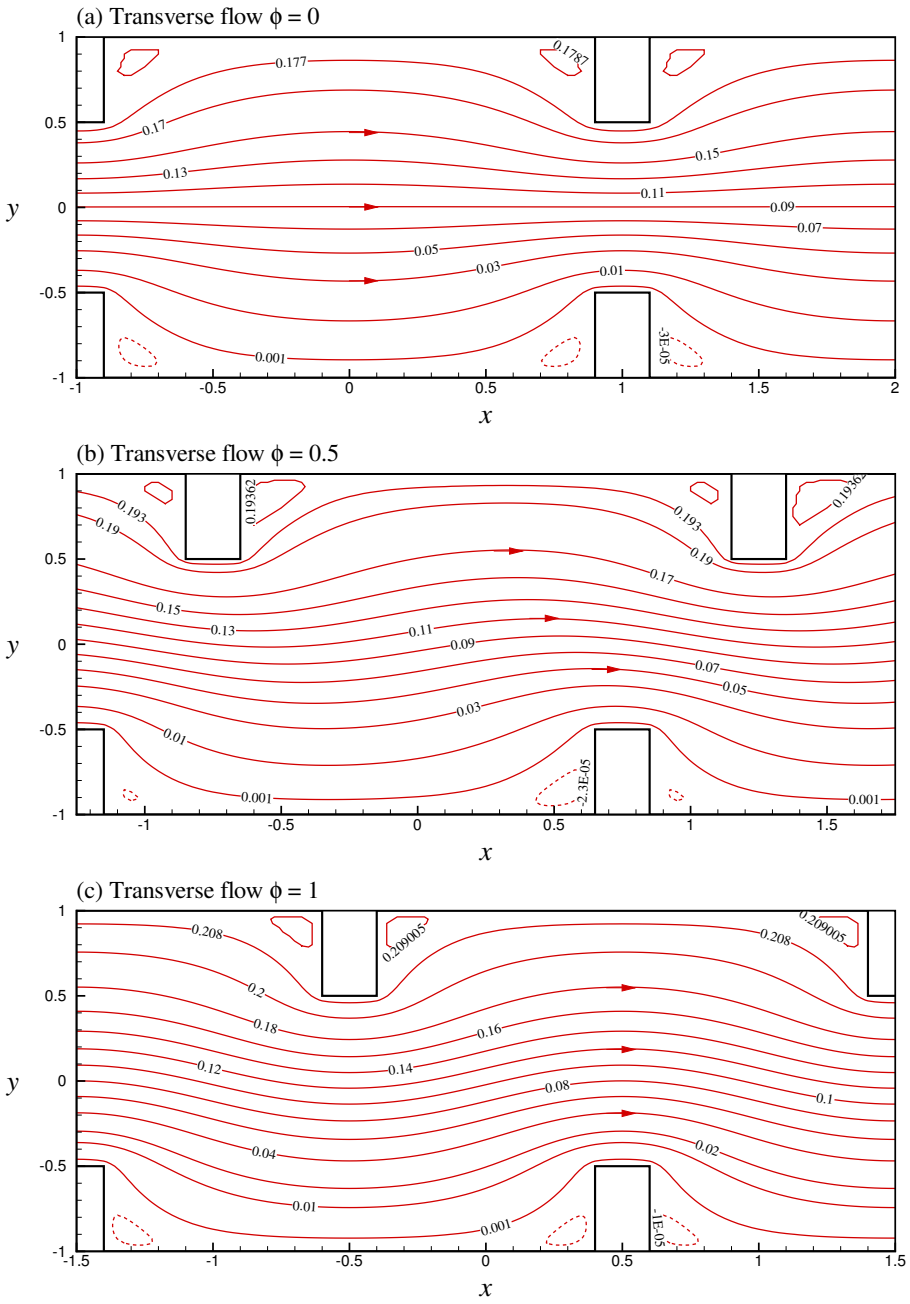

Figure 4: Streamlines for transverse flow, with phase shift (a) $\phi = 0$, (b) $\phi = 0.5$, (c) $\phi = 1$, where $a = 0.9$, and $b = h = 0.5$. The stream function is set to be zero on the lower wall.

For longitudinal flow, the alignment of grooves means the formation of the widest possible rectangular cross-sectional region without a rib in one period width of the channel; see figure 3(a). This widest possible region without a rib, which has the dimensions of $2a$ by $2(h+b)$, allows the flow to attain a peak velocity at its center. It is because, under this symmetric configuration, the interior of this region is subject to the least possible boundary friction due to the neighboring ribs. When the phase shift increases to $\phi = 0.5$ (figure 3(b)), not only is this region smaller in extent, but also the peak velocity is smaller in magnitude. When the two patterns are completely out of phase, $\phi = 1$ (figure 3(c)), this region with a center peak velocity will lose its identity after merging with the adjacent ones, forming a nearly uniform flow along the centerline of the channel. In this example, one can see that the peak velocity reduces by more than 10% as ϕ varies from 0 to 1. Some of these flow features have been reported previously by Mohammadi and Floryan (2013b, 2013a, 2015).

For transverse flow, the alignment of ribs means the formation of the narrowest possible cross section of the channel; see figure 4(a). This of course amounts to the largest possible flow resistance for the same wall pattern. Opposite to the case of longitudinal flow, the transverse flow along the centerline of the channel attains the maximum velocity at the point between the centers of opposite ribs, and the minimum velocity between the centers of opposite grooves. The narrow cross section between opposite ribs will widen up as the phase shift increases to an extent where the ribs are no longer directly opposite to each other. As a consequence, the flow rate will increase as the phase shift increases for flow transverse to the pattern; see figures 4(b, c). In this example, one can get from the topmost stream function value that the flow rate $q_\perp$ increases by some 18% as ϕ varies from 0 to 1. While most of the flow goes forward in the grooves, recirculation occurs in the corners between the groove base and the ribs. In shallow grooves, these corner eddies are small in extent and weak in strength. In deeper grooves, the recirculation zone may grow in extent such that a string of Moffatt eddies of alternate sense and decreasing strength is formed (Wang 2003).

We further show in figure 5 how the effective slip lengths $\lambda_\parallel$ and $\lambda_\perp$ may vary with the phase shift for various values of a, where $b = 0.5$ and $h = 0.5, 0.05$. Again, we see that the effective longitudinal slip length will decrease as the phase shift varies from 0 to 1. In contrast, the effective transverse slip length, especially for thin ribs, will appreciably increase

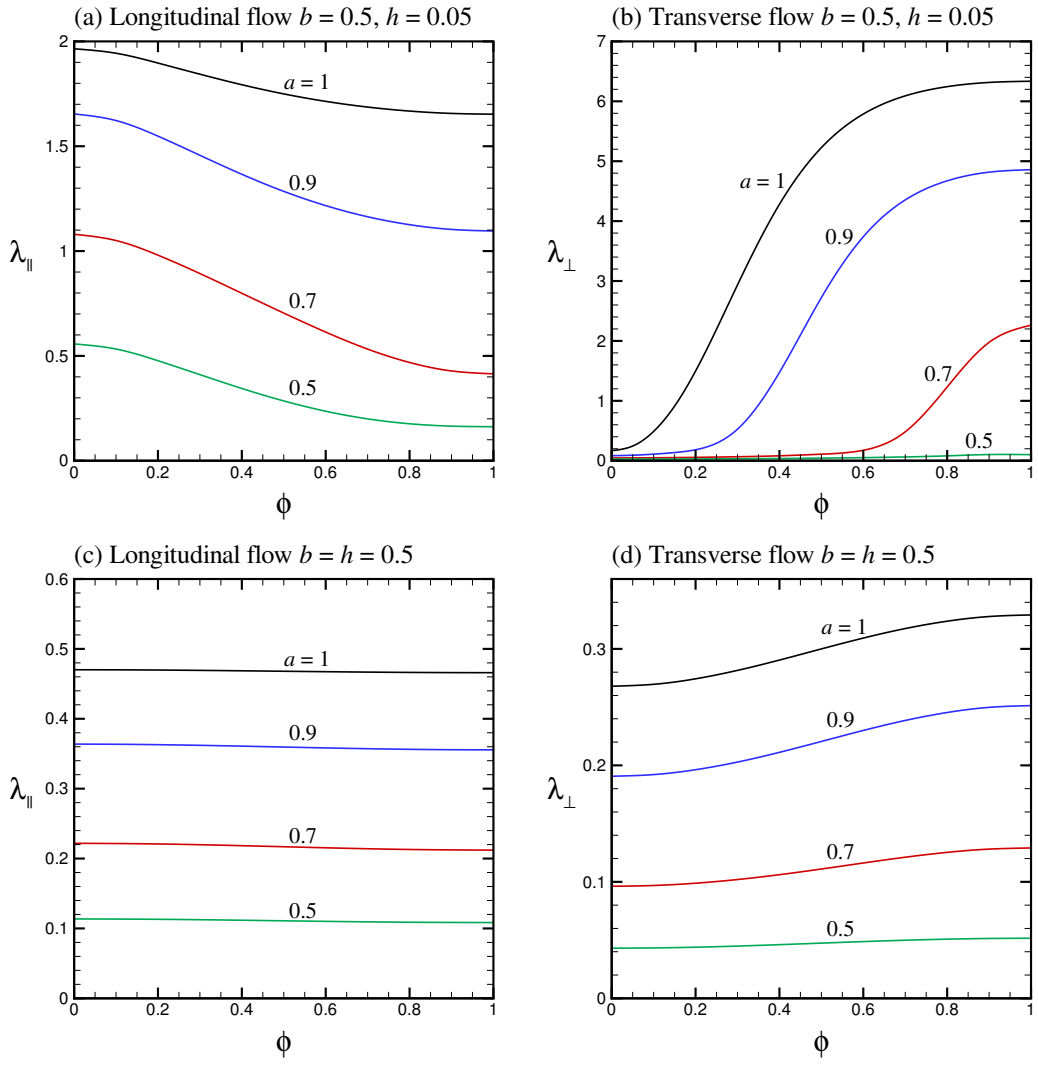

Figure 5: Effective slip lengths, $\lambda_{\parallel}$ and $\lambda_{\perp}$, as functions of the phase shift ϕ, for various values of a and $b = 0.5$, where $h = 0.05$ in (a, b), and $h = 0.5$ in (c, d).

as the phase shift changes from 0 to 1. These changes are much more pronounced in the case of a narrow channel. The results further confirm that, for thin ribs in a narrow channel, transverse flow is much more sensitive to the phase shift than longitudinal flow.

We next show in figure 6 the effect of the groove depth b on the effective slip lengths. The slip lengths will increase monotonically with the groove depth, but such increase will gradually diminish as the grooves become sufficiently deep. This is manifested by the leveling off of the curves shown in the figure. For longitudinal thin fins in a narrow channel $h = 0.5$, a large groove depth $b \sim 10$ is needed in order to reach the deep-groove limit; see figure 6(a). For transverse ribs, thin or thick, and a narrow channel, a much shallower groove depth $b \sim 1$ is needed in order to attain the deep-groove limit; see figure 6(b). In a thicker channel $h = 2$, the deep-groove limits can be practically reached when $b \sim 2$ in all cases; see figure 6(c, d). In the limiting case of an infinitely thick channel $h \gg 1$, our problem reduces to the one studied by Wang (2003), i.e. flow over a grooved surface. Figure 6(e) shows $\lambda_\parallel$ as a function of a and b for $h = \infty$. These results for the longitudinal slip length can be checked to agree exactly with those presented in figure 4 of Wang (2003). In this case, the deep-groove limit can be computed using the analytical formula deduced by Richardson (1971):

$$\lambda_\parallel \to \frac{(1-a)\ln(1-a) + (1+a)\ln(1+a)}{\pi} \qquad \text{as } b,\, h \to \infty. \tag{45}$$

These limits can be practically attained when $b \sim 2$, as shown in figure 6(e).

We also show in figure 6(f) the transverse slip length $\lambda_\perp$ as a function of a and b for $h \to \infty$. Wang (2003) presented a similar plot in his figure 5, which, however, needs correction. The correction arises from an error in expressing one of the coefficients.[2] Some corrections that should be made to Wang (2003) are noted in Appendix III. Our results show that the transverse slip length $\lambda_\perp$ for thin fins, $a = 1$, can practically attain the deep-groove limit of 0.1772 (Jeong 2001) when $b \sim 2$. Wang (2003) failed to obtain results that could tend to this asymptotic value. Our figure 6(f) should supersede figure 5 of Wang (2003).

Finally, we show in figure 7 the effect of the channel height h on the slip lengths. In all cases, the effective slip lengths, $\lambda_\parallel$ and $\lambda_\perp$, will basically decrease as the distance between the two walls increases (except for very small h and $\phi = 0$ where $\lambda_\perp$ may slightly increase

[2]Private communication between Professor C.Y. Wang and the author.

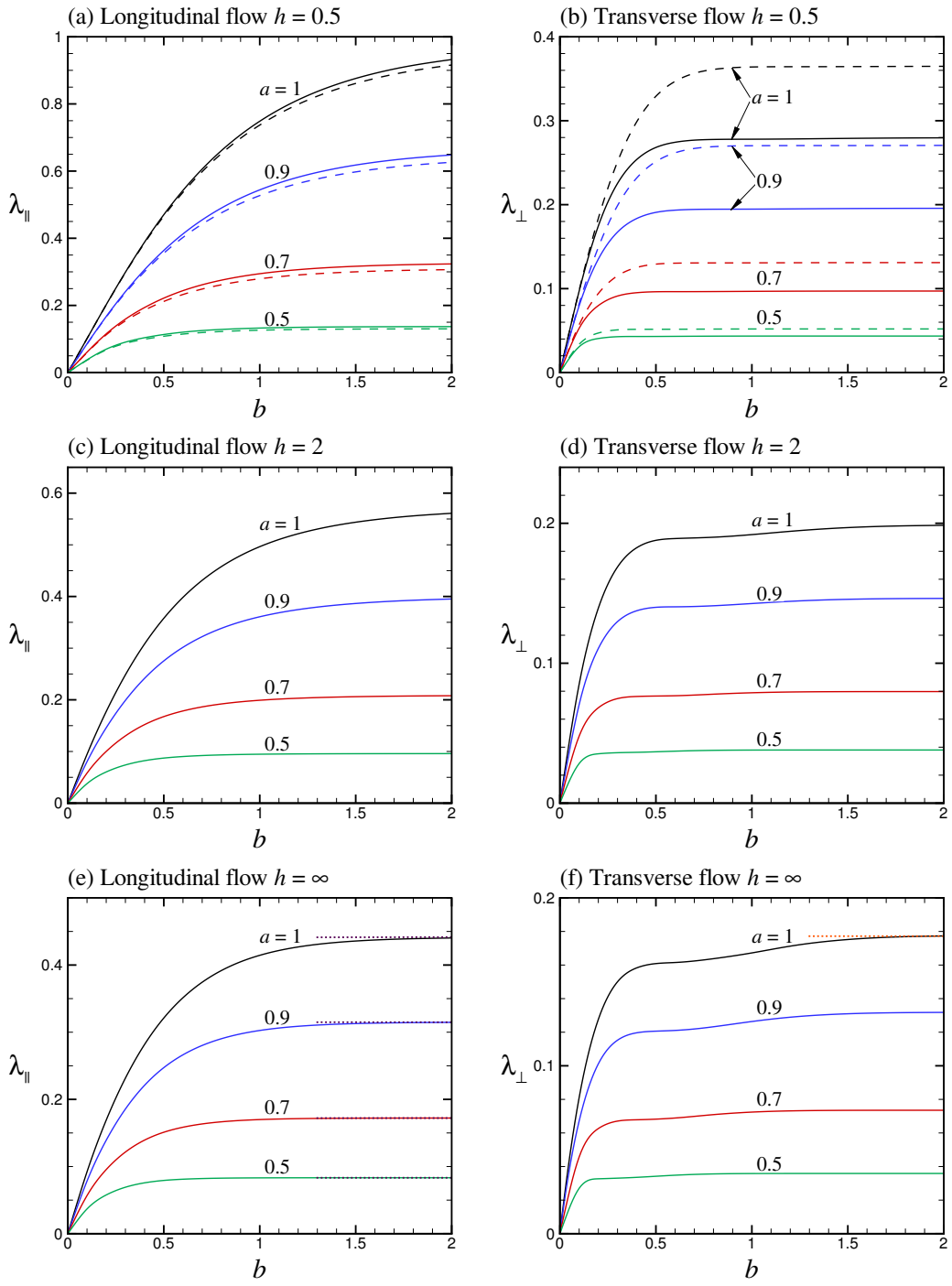

Figure 6: Effective slip lengths, $\lambda_{\parallel}$ and $\lambda_{\perp}$, as functions of the groove depth b for various values of a, where $h = 0.5$, 2, ∞. The solid and dashed lines are for $\phi = 0$, 1, respectively. The dotted lines in (e) are from equation (45). The dotted line in (f) is from Jeong (2001).

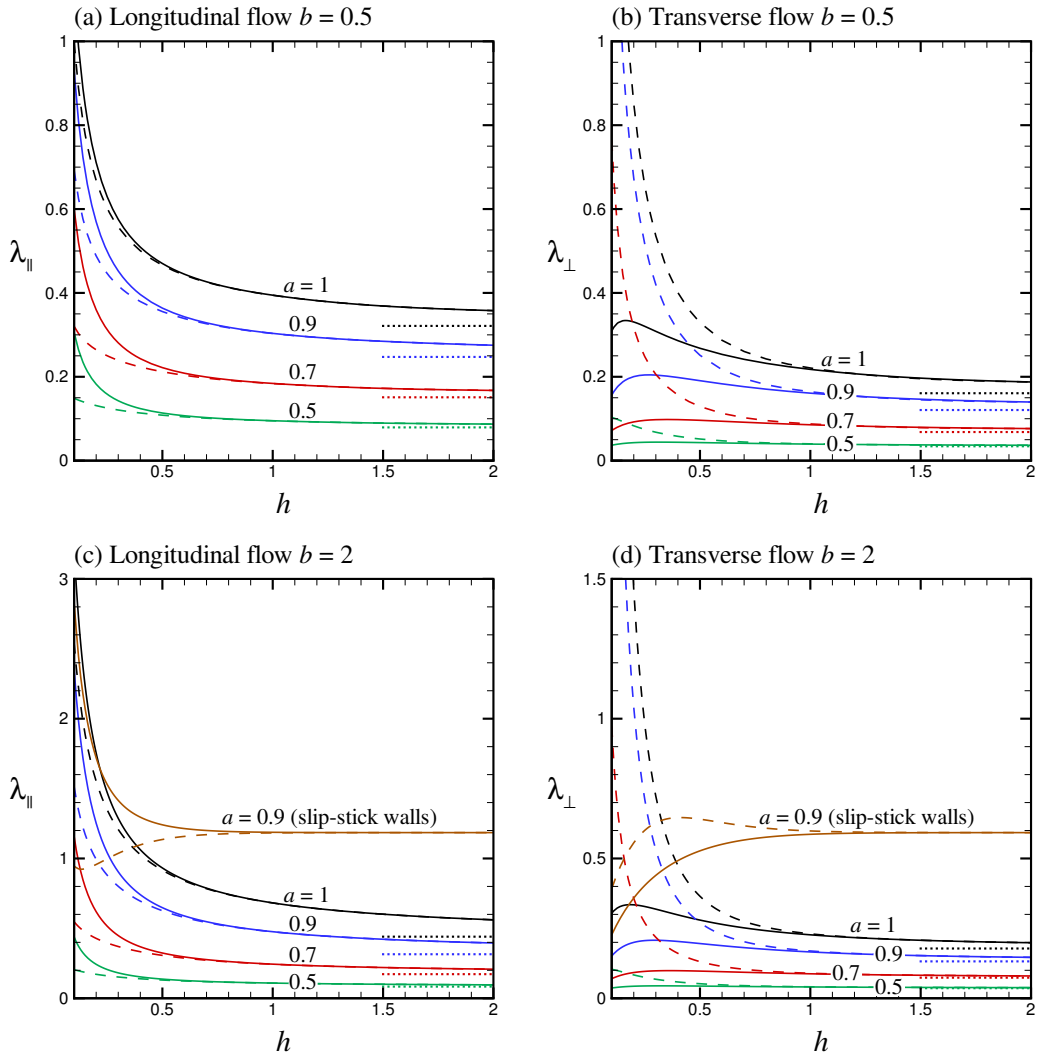

Figure 7: Effective slip lengths, $\lambda_\parallel$ and $\lambda_\perp$, as functions of the channel height h for various values of a, where $b = 0.5$, 2. The solid and dashed lines are for $\phi = 0$, 1, respectively. The dotted lines are the asymptotes for $h \to \infty$. In (c, d), the effective slip lengths for flow through a channel bounded by superhydrophobic slip–stick walls of area fraction of perfect slip $a = 0.9$ are presented.

as h increases). In other words, the channel confinement may have a favorable effect on both $\lambda_\parallel$ and $\lambda_\perp$, irrespective of the phase shift. These trends are somewhat different from those that have been observed for superhydrophobic surfaces. In a channel bounded by slip–stick superhydrophobic walls, increasing the channel confinement (i.e. decreasing the channel height) may increase the longitudinal slip length but decrease the transverse slip length when the patterns are in phase. The opposite is true when the patterns are half a period out of phase (except for very small h) (Cheng et al. 2009, Ng and Chen 2013).

In figure 7, it is clearly seen that the phase shift will have significant effect on the flow, irrespective of the flow direction and other geometrical parameters, only when $h < 1$, i.e. when the distance between the two walls is smaller than one period length of the wall pattern. This figure also confirms our earlier observation that, in a narrow channel, the phase shift can have much more significant effect on the transverse flow than on the longitudinal flow. Here, we see that, for $h < 0.5$, $\lambda_\perp$ can dramatically increase by several multiples when ϕ changes from 0 to 1. Nevertheless, under the same condition, the effective slip length is in general larger in the longitudinal direction than in the transverse direction. This is expected since longitudinal flow is in general subject to smaller resistance than transverse flow. In this figure, we also show the asymptotic slip lengths for $h \gg 1$, corresponding to the limiting values when the effect due to channel wall confinement vanishes or the effective slip lengths for flow over a grooved surface, as has been considered by Wang (2003). We have found that these thick-channel (or single-surface) limits will not be attained until the channel height is sufficiently large, which can range from $O(10)$ to $O(10^3)$, depending on a and b. The larger a and b, the thicker the channel is needed for the wall confinement effect to be negligible. In other words, the effective slip lengths for flow bounded by grooved walls, where the grooves are deep and wide, do not get close to those for flow over a single grooved surface until the walls are separated by a distance that is several orders of magnitude larger than the period length of the grooves. This suggests that in practice channel wall confinement should be taken into account when evaluating the effective slip length for a patterned surface. We also show in figure 7(c, d) the effective slip lengths for flow through a channel bounded by superhydrophobic slip–stick walls, as has been considered by Ng and Chen (2013). Except when h is very small, the effective slip length for flow bounded by slip–stick walls can be

several times larger than the corresponding slip length for flow bounded by grooved walls.

4 Concluding remarks

We have shown that, for Stokes flow between two grooved surfaces, the phase difference between grooves on the two surfaces may have opposite effects on the effective slip length for parallel and cross flows. For parallel flow, increasing the phase shift may decrease the flow rate and effective slip length, but such change is relatively mild. In sharp contrast, for cross flow, increasing the phase shift may increase the flow rate and effective slip length, and such change can be very dramatic. In a channel with thin ribs, flow parallel to the grooves is rate-controlled by flow in the widest cross sectional region without a rib, while flow transverse to the grooves is rate-limited by the narrowest cross sectional region between opposite ribs. In all cases, the significance of the phase shift is, however, limited to narrow channels, where the channel height is not larger than the period of the wall pattern. On the other hand, the effective slip lengths for wall-bounded flow are in general larger than the thick-channel asymptotic limits corresponding to slip lengths for flow over a single grooved surface. These thick-channel limiting values are not practically attained until the channel height is much larger, as large as three orders of magnitude, than the wall pattern period length. These results suggest that, in a channel where the ratio of channel height to period length is only moderately large, the effect due to the phase shift is probably negligible, but that due to the wall confinement has to be taken into account when the effective slip lengths are evaluated. The last statement is valid especially for surfaces with deep and wide grooves.

Acknowledgements

Financial support was given by the Research Grants Council of the Hong Kong Special Administrative Region, China, through General Research Fund Project No. 17206615.

Appendix I: Flow through an equivalent uniform channel with boundary slip

Poiseuille flow through a slit channel of height $2h$ and constant slip length λ at the walls, as depicted in figure 8, has the following velocity profile:

$$u(y) = \frac{h^2}{2}\left[1 - \left(\frac{y}{h}\right)^2 + \frac{2\lambda}{h}\right], \tag{A 1}$$

which satisfies the partial slip condition at the upper/lower walls:

$$u = \mp\lambda\frac{\mathrm{d}u}{\mathrm{d}y} \qquad \text{at } y = \pm h. \tag{A 2}$$

The flow rate per unit spanwise width of the channel is therefore

$$q = \int_{-h}^{h} u\mathrm{d}y = \frac{2h^3}{3} + 2\lambda h^2. \tag{A 3}$$

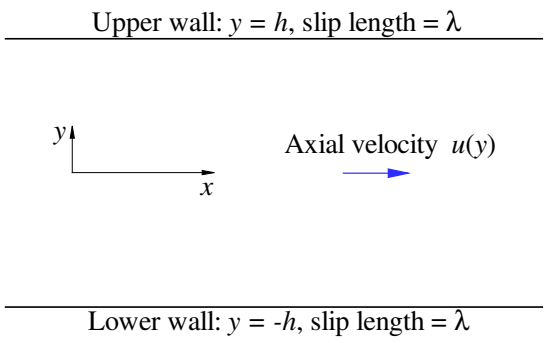

Figure 8: Flow through a slit channel with partial slip at the walls.

Appendix II: Equations for the coefficients in the case of transverse flow

On integrating equation (35) with respect to x from $-1-\phi/2$ to $1-\phi/2$ (or x' from -1 to 1), we get

$$\begin{aligned} A_0 &= \sum_{n=1}^{N} \frac{(-1)^{n+1}}{\beta_n} \left[\left(1+e^{-2\beta_n b}\right) E_n + (1+\beta_n b) F_n + (1-\beta_n b) e^{-\beta_n b} G_n \right] \\ &\quad + \sum_{n=1}^{P} \frac{1-2\sigma_n a \,\mathrm{csch}(2\sigma_n a)}{\sigma_n^2 a} Q_n. \end{aligned} \tag{A 4}$$

Multiplying equation (35) by $\cos(\alpha_m x)$, followed by integration with respect to x from $-1-\phi/2$ to $1-\phi/2$, we get

$$\begin{aligned} & A_m + [1+\alpha_m h \tanh(\alpha_m h)]\, B_m \\ & \quad - \sum_{n=1}^{N} I_{mn}^{(1)} \left[\left(1+e^{-2\beta_n b}\right) E_n + (1+\beta_n b) F_n + (1-\beta_n b) e^{-\beta_n b} G_n \right] \\ & \quad - \sum_{n=1}^{N} I_{mn}^{(2)} \left[\left(1+e^{-2\gamma_n b}\right) H_n + (1+\gamma_n b) K_n + (1-\gamma_n b) e^{-\gamma_n b} L_n \right] \\ & \quad - \sum_{n=1}^{P} \left[J_{mn}^{(1)} Q_n + J_{mn}^{(2)} R_n \right] = 0, \qquad m = 1, \cdots, M, \end{aligned} \tag{A 5}$$

where $I_{mn}^{(1)}$ and $I_{mn}^{(2)}$ are given by equations (11) and (12), and

$$\begin{aligned} J_{mn}^{(1)} &= \frac{2\cos(\alpha_m \phi/2)}{a\left(\alpha_m^2+\sigma_n^2\right)^2} \Big\{ 2\alpha_m \sigma_n \coth(\sigma_n a) \sin(\alpha_m a) \\ &\quad - \left[\alpha_m^2 - \sigma_n^2 + 2\sigma_n a \left(\alpha_m^2+\sigma_n^2\right) \mathrm{csch}(2\sigma_n a) \right] \cos(\alpha_m a) \Big\}, \end{aligned} \tag{A 6}$$

$$\begin{aligned} J_{mn}^{(2)} &= \frac{2\sin(\alpha_m \phi/2)}{a\left(\alpha_m^2+\sigma_n^2\right)^2} \Big\{ \left[-\alpha_m^2 + \sigma_n^2 + 2\sigma_n a \left(\alpha_m^2+\sigma_n^2\right) \mathrm{csch}(2\sigma_n a) \right] \sin(\alpha_m a) \\ &\quad - 2\alpha_m \sigma_n \tanh(\sigma_n a) \cos(\alpha_m a) \Big\}. \end{aligned} \tag{A 7}$$

Multiplying equation (35) by $\sin(\alpha_m x)$, followed by integration with respect to x from $-1-\phi/2$ to $1-\phi/2$, we get

$$\begin{aligned} & \tanh(\alpha_m h) C_m + [\alpha_m h + \tanh(\alpha_m h)]\, D_m \\ & \quad - \sum_{n=1}^{N} I_{mn}^{(3)} \left[\left(1+e^{-2\beta_n b}\right) E_n + (1+\beta_n b) F_n + (1-\beta_n b) e^{-\beta_n b} G_n \right] \end{aligned}$$

$$
\begin{aligned}
&- \sum_{n=1}^{N} I_{mn}^{(4)} \left[\left(1 + e^{-2\gamma_n b}\right) H_n + (1+\gamma_n b) K_n + (1-\gamma_n b) e^{-\gamma_n b} L_n \right] \\
&- \sum_{n=1}^{P} \left[J_{mn}^{(3)} Q_n + J_{mn}^{(4)} R_n \right] = 0, \qquad m = 1, \cdots, M,
\end{aligned} \tag{A 8}
$$

where $I_{mn}^{(3)}$ and $I_{mn}^{(4)}$ are given by equations (14) and (15), and

$$
\begin{aligned}
J_{mn}^{(3)} &= \frac{2\sin(\alpha_m \phi/2)}{a\left(\alpha_m^2 + \sigma_n^2\right)^2} \Big\{ -2\alpha_m \sigma_n \coth(\sigma_n a) \sin(\alpha_m a) \\
&\quad + \left[\alpha_m^2 - \sigma_n^2 + 2\sigma_n a \left(\alpha_m^2 + \sigma_n^2\right) \operatorname{csch}(2\sigma_n a) \right] \cos(\alpha_m a) \Big\},
\end{aligned} \tag{A 9}
$$

$$
\begin{aligned}
J_{mn}^{(4)} &= \frac{2\cos(\alpha_m \phi/2)}{a\left(\alpha_m^2 + \sigma_n^2\right)^2} \Big\{ \left[-\alpha_m^2 + \sigma_n^2 + 2\sigma_n a \left(\alpha_m^2 + \sigma_n^2\right) \operatorname{csch}(2\sigma_n a) \right] \sin(\alpha_m a) \\
&\quad - 2\alpha_m \sigma_n \tanh(\sigma_n a) \cos(\alpha_m a) \Big\}.
\end{aligned} \tag{A 10}
$$

Multiplying equation (36) by $\sin(\alpha_m x)$, followed by integration with respect to x from $-1 - \phi/2$ to $1 - \phi/2$, we get

$$
\begin{aligned}
&\tanh(\alpha_m h) A_m + \alpha_m h B_m \\
&\quad + \sum_{n=1}^{N} I_{mn}^{(5)} \left[\left(1 - e^{-2\beta_n b}\right) E_n + \beta_n b F_n + \beta_n b e^{-\beta_n b} G_n \right] \\
&\quad - \sum_{n=1}^{N} I_{mn}^{(6)} \left[\left(1 - e^{-2\gamma_n b}\right) H_n + \gamma_n b K_n + \gamma_n b e^{-\gamma_n b} L_n \right] = 0, \qquad m = 1, \cdots, M,
\end{aligned} \tag{A 11}
$$

where

$$
I_{mn}^{(5)} = \cos(\alpha_m \phi/2) \times \begin{cases} \left(\frac{\sin[(\alpha_m - \beta_n)a]}{\alpha_m - \beta_n} - \frac{\sin[(\alpha_m + \beta_n)a]}{\alpha_m + \beta_n} \right) & \text{for } \alpha_m \neq \beta_n \\ a & \text{for } \alpha_m = \beta_n \end{cases}, \tag{A 12}
$$

$$
I_{mn}^{(6)} = -\sin(\alpha_m \phi/2) \times \begin{cases} \left(\frac{\sin[(\alpha_m - \gamma_n)a]}{\alpha_m - \gamma_n} + \frac{\sin[(\alpha_m + \gamma_n)a]}{\alpha_m + \gamma_n} \right) & \text{for } \alpha_m \neq \gamma_n \\ a & \text{for } \alpha_m = \gamma_n \end{cases}. \tag{A 13}
$$

Multiplying equation (36) by $\cos(\alpha_m x)$, followed by integration with respect to x from $-1 - \phi/2$ to $1 - \phi/2$, we get

$$
\begin{aligned}
&C_m + \alpha_m h \tanh(\alpha_m h) D_m \\
&\quad - \sum_{n=1}^{N} I_{mn}^{(7)} \left[\left(1 - e^{-2\beta_n b}\right) E_n + \beta_n b F_n + \beta_n b e^{-\beta_n b} G_n \right] \\
&\quad + \sum_{n=1}^{N} I_{mn}^{(8)} \left[\left(1 - e^{-2\gamma_n b}\right) H_n + \gamma_n b K_n + \gamma_n b e^{-\gamma_n b} L_n \right] = 0, \qquad m = 1, \cdots, M,
\end{aligned} \tag{A 14}
$$

where

$$I_{mn}^{(7)} = \sin(\alpha_m \phi/2) \times \begin{cases} \left(\frac{\sin[(\alpha_m - \beta_n)a]}{\alpha_m - \beta_n} - \frac{\sin[(\alpha_m + \beta_n)a]}{\alpha_m + \beta_n} \right) & \text{for } \alpha_m \neq \beta_n \\ a & \text{for } \alpha_m = \beta_n \end{cases}, \tag{A 15}$$

$$I_{mn}^{(8)} = \cos(\alpha_m \phi/2) \times \begin{cases} \left(\frac{\sin[(\alpha_m - \gamma_n)a]}{\alpha_m - \gamma_n} + \frac{\sin[(\alpha_m + \gamma_n)a]}{\alpha_m + \gamma_n} \right) & \text{for } \alpha_m \neq \gamma_n \\ a & \text{for } \alpha_m = \gamma_n \end{cases}. \tag{A 16}$$

Multiplying equation (37) by $\cos(\beta_m x')$, followed by integration with respect to x' from $-a$ to a, we get

$$\begin{aligned} &\sum_{n=1}^{M} I_{nm}^{(1)} \alpha_n \{A_n + [\alpha_n h + 2\tanh(\alpha_n h)] B_n\} \\ &\quad + \sum_{n=1}^{M} I_{nm}^{(3)} \alpha_n \{C_n + [2 + \alpha_n h \tanh(\alpha_n h)] D_n\} \\ &\quad + \beta_m a \left\{ \left(1 - e^{-2\beta_m b}\right) E_m + (2 + \beta_m b) F_m - (2 - \beta_m b) e^{-\beta_m b} G_m \right\} \\ &\quad = (-1)^{m+1} \frac{2h}{\beta_m}, \qquad m = 1, \cdots, N. \end{aligned} \tag{A 17}$$

Multiplying equation (37) by $\sin(\gamma_m x')$, followed by integration with respect to x' from $-a$ to a, we get

$$\begin{aligned} &\sum_{n=1}^{M} I_{nm}^{(2)} \alpha_n \{A_n + [\alpha_n h + 2\tanh(\alpha_n h)] B_n\} \\ &\quad + \sum_{n=1}^{M} I_{nm}^{(4)} \alpha_n \{C_n + [2 + \alpha_n h \tanh(\alpha_n h)] D_n\} \\ &\quad + \gamma_m a \left\{ \left(1 - e^{-2\gamma_m b}\right) H_m + (2 + \gamma_m b) K_m - (2 - \gamma_m b) e^{-\gamma_m b} L_m \right\} \\ &\quad = 0, \qquad m = 1, \cdots, N. \end{aligned} \tag{A 18}$$

Multiplying equation (38) by $\cos(\beta_m x')$, followed by integration with respect to x' from $-a$ to a, we get

$$\begin{aligned} &\sum_{n=1}^{M} I_{nm}^{(1)} \alpha_n^2 \{A_n + [3 + \alpha_n h \tanh(\alpha_n h)] B_n\} \\ &\quad + \sum_{n=1}^{M} I_{nm}^{(3)} \alpha_n^2 \{C_n + [\alpha_n h + 3\tanh(\alpha_n h)] D_n\} \\ &\quad - \beta_m^2 a \left\{ \left(1 + e^{-2\beta_m b}\right) E_m + (3 + \beta_m b) F_m + (3 - \beta_m b) e^{-\beta_m b} G_m \right\} \\ &\quad + \sum_{n=1}^{P} J_{mn}^{(5)} \sigma_n^2 Q_n = (-1)^{m+1} \frac{2}{\beta_m}, \qquad m = 1, \cdots, N, \end{aligned} \tag{A 19}$$

where

$$J_{mn}^{(5)} = (-1)^{m+1} \frac{4\beta_m \sigma_n \coth(\sigma_n a)}{a\left(\beta_m^2 + \sigma_n^2\right)^2}. \tag{A 20}$$

Multiplying equation (38) by $\sin(\gamma_m x')$, followed by integration with respect to x' from $-a$ to a, we get

$$\begin{aligned}
&\sum_{n=1}^{M} I_{nm}^{(2)} \alpha_n^2 \left\{A_n + [3 + \alpha_n h \tanh(\alpha_n h)] B_n\right\} \\
&\quad + \sum_{n=1}^{M} I_{nm}^{(4)} \alpha_n^2 \left\{C_n + [\alpha_n h + 3\tanh(\alpha_n h)] D_n\right\} \\
&\quad - \gamma_m^2 a \left\{\left(1 + e^{-2\gamma_m b}\right) H_m + (3 + \gamma_m b) K_m + (3 - \gamma_m b) e^{-\gamma_m b} L_m\right\} \\
&\quad + \sum_{n=1}^{P} J_{mn}^{(6)} \sigma_n^2 R_n = 0, \qquad m = 1, \cdots, N,
\end{aligned} \tag{A 21}$$

where

$$J_{mn}^{(6)} = (-1)^{m+1} \frac{4\gamma_m \sigma_n \tanh(\sigma_n a)}{a\left(\gamma_m^2 + \sigma_n^2\right)^2}. \tag{A 22}$$

Multiplying equation (39) by $\cos(\beta_m x')$, followed by integration with respect to x' from $-a$ to a, we get

$$a\left(2e^{-\beta_m b} E_m + e^{-\beta_m b} F_m + G_m\right) + \sum_{n=1}^{P} J_{mn}^{(5)} (-1)^n Q_n = 0, \qquad m = 1, \cdots, N. \tag{A 23}$$

Multiplying equation (39) by $\sin(\gamma_m x')$, followed by integration with respect to x' from $-a$ to a, we get

$$a\left(2e^{-\gamma_m b} H_m + e^{-\gamma_m b} K_m + L_m\right) + \sum_{n=1}^{P} J_{mn}^{(6)} (-1)^n R_n = 0, \qquad m = 1, \cdots, N. \tag{A 24}$$

Multiplying equation (40) by $\sin(\sigma_m y')$, followed by integration with respect to y' from $-b$ to 0, we get

$$\begin{aligned}
&\sum_{n=1}^{N} (-1)^{n+1} \left[K_{mn}^{(1)} E_n + K_{mn}^{(2)} F_n + K_{mn}^{(3)} G_n\right] \\
&\quad + \frac{b}{2} \left[-\tanh(\sigma_m a) + \coth(\sigma_m a) + 1/(\sigma_m a)\right] Q_m = 0, \qquad m = 1, \cdots, P,
\end{aligned} \tag{A 25}$$

$$\begin{aligned}
&\sum_{n=1}^{N} (-1)^{n+1} \left[K_{mn}^{(4)} H_n + K_{mn}^{(5)} K_n + K_{mn}^{(6)} L_n\right] \\
&\quad + \frac{b}{2} \left[-\coth(\sigma_m a) + \tanh(\sigma_m a) + 1/(\sigma_m a)\right] R_m = 0, \qquad m = 1, \cdots, P,
\end{aligned} \tag{A 26}$$

where

$$K_{mn}^{(1)} = \frac{\sigma_m \left(e^{-2\beta_n b} - 1\right)}{\sigma_m^2 + \beta_n^2}, \tag{A 27}$$

$$K_{mn}^{(2)} = \frac{\sigma_m \beta_n \left[2\beta_n - (\sigma_m^2 + \beta_n^2)\, b + (-1)^{m+1} 2\beta_n e^{-\beta_n b}\right]}{(\sigma_m^2 + \beta_n^2)^2}, \tag{A 28}$$

$$K_{mn}^{(3)} = \frac{\sigma_m \beta_n \left\{(-1)^m 2\beta_n - \left[(\sigma_m^2 + \beta_n^2)\, b + 2\beta_n\right] e^{-\beta_n b}\right\}}{(\sigma_m^2 + \beta_n^2)^2}, \tag{A 29}$$

$$K_{mn}^{(4)} = \frac{\sigma_m \left(e^{-2\gamma_n b} - 1\right)}{\sigma_m^2 + \gamma_n^2}, \tag{A 30}$$

$$K_{mn}^{(5)} = \frac{\sigma_m \gamma_n \left[2\gamma_n - (\sigma_m^2 + \gamma_n^2)\, b + (-1)^{m+1} 2\gamma_n e^{-\gamma_n b}\right]}{(\sigma_m^2 + \gamma_n^2)^2}, \tag{A 31}$$

$$K_{mn}^{(6)} = \frac{\sigma_m \gamma_n \left\{(-1)^m 2\gamma_n - \left[(\sigma_m^2 + \gamma_n^2)\, b + 2\gamma_n\right] e^{-\gamma_n b}\right\}}{(\sigma_m^2 + \gamma_n^2)^2}. \tag{A 32}$$

Equations (A 5), (A 8), (A 11), (A 14), (A 17), (A 18), (A 19), (A 21), (A 23), (A 24), (A 25) and (A 26) constitute a system of $4M + 6N + 2P$ equations that can be solved for the same number of unknown coefficients: $A_{1,\cdots,M}$, $B_{1,\cdots,M}$, $C_{1,\cdots,M}$, $D_{1,\cdots,M}$, $E_{1,\cdots,N}$, $F_{1,\cdots,N}$, $G_{1,\cdots,N}$, $H_{1,\cdots,N}$, $K_{1,\cdots,N}$, $L_{1,\cdots,N}$, $Q_{1,\cdots,P}$, and $R_{1,\cdots,P}$. We have again used the routine IMSL-DLSARG to solve the system of equations.

Appendix III: Corrections for Wang (2003)

The following equation numbers and notations are those in Wang (2003). Equation (32) should read

$$\begin{aligned} J_{mn} \;=\; & \left\{2\beta_n\gamma_m \left(1 + e^{-2\beta_n a}\right)^2 \sin(a\gamma_m) + \left[\left(\beta_n^2 - \gamma_m^2\right)\left(1 - e^{-4\beta_n a}\right)\right.\right. \\ & \left.\left. - 4\beta_n a \left(\beta_n^2 + \gamma_m^2\right) e^{-2\beta_n a}\right] \cos(a\gamma_m)\right\} / \left[a \left(1 - e^{-2\beta_n a}\right) \left(\beta_n^2 + \gamma_m^2\right)^2\right]. \end{aligned}$$

In equation (21), $e^{-2\beta_n}$ should read $e^{-2\beta_n a}$, while in equations (27) and (28), $C_n b e^{-2\alpha_n b}$ should read $C_n b e^{-\alpha_n b}$.

References

Beavers, G. S. and Joseph, D. D. (1967). Boundary conditions at a naturally permeable wall, *J. Fluid Mech.* **30**(01): 197–207.

Cheng, Y. P., Teo, C. J. and Khoo, B. C. (2009). Microchannel flows with superhydrophobic surfaces: Effects of Reynolds number and pattern width to channel height ratio, *Phys. Fluids* **21**(12): 122004.

Choi, C.-H., Westin, K. J. A. and Breuer, K. S. (2003). Apparent slip flows in hydrophilic and hydrophobic microchannels, *Phys. Fluids* **15**(10): 2897–2902.

Jeong, J.-T. (2001). Slip boundary condition on an idealized porous wall, *Phys. Fluids* **13**(7): 1884–1890.

Luchini, P., Manzo, F. and Pozzi, A. (1991). Resistance of a grooved surface to parallel flow and cross-flow, *J. Fluid Mech.* **228**: 87–109.

Maynes, D., Jeffs, K., Woolford, B. and Webb, B. (2007). Laminar flow in a microchannel with hydrophobic surface patterned microribs oriented parallel to the flow direction, *Phys. Fluids* **19**(9): 093603.

Mohammadi, A. and Floryan, J. M. (2012). Mechanism of drag generation by surface corrugation, *Phys. Fluids* **24**(1): 013602.

Mohammadi, A. and Floryan, J. M. (2013a). Groove optimization for drag reduction, *Phys. Fluids* **25**(11): 113601.

Mohammadi, A. and Floryan, J. M. (2013b). Pressure losses in grooved channels, *J. Fluid Mech.* **725**: 23–54.

Mohammadi, A. and Floryan, J. M. (2015). Numerical analysis of laminar-drag-reducing grooves, *ASME J. Fluids Eng.* **137**(4): 041201.

Ng, C.-O. and Chen, B. (2013). Microchannel flows with superhydrophobic surfaces: Effects of phase shift of wall patterns, *Proceedings of the 14th Asian Congress of Fluid Mechanics*, pp. 1037–1041.

Ng, C.-O., Chu, H. C. and Wang, C.-Y. (2010). On the effects of liquid-gas interfacial shear on slip flow through a parallel-plate channel with superhydrophobic grooved walls, *Phys. Fluids* **22**(10): 102002.

Ng, C.-O. and Wang, C.-Y. (2009). Stokes shear flow over a grating: Implications for superhydrophobic slip, *Phys. Fluids* **21**(1): 013602.

Ng, C.-O. and Zhou, Q. (2012). Electro-osmotic flow through a thin channel with gradually varying wall potential and hydrodynamic slippage, *Fluid Dyn. Res.* **44**(5): 055507.

Ou, J., Perot, B. and Rothstein, J. P. (2004). Laminar drag reduction in microchannels using ultrahydrophobic surfaces, *Phys. Fluids* **16**(12): 4635–4643.

Philip, J. R. (1972). Flows satisfying mixed no-slip and no-shear conditions, *ZAMP* **23**(3): 353–372.

Richardson, S. (1971). A model for the boundary condition of a porous material. part 2, *J. Fluid Mech.* **49**(02): 327–336.

Smith, J. D., Dhiman, R., Anand, S., Reza-Garduno, E., Cohen, R. E., McKinley, G. H. and Varanasi, K. K. (2013). Droplet mobility on lubricant-impregnated surfaces, *Soft Matter* **9**(6): 1772–1780.

Teo, C. J. and Khoo, B. C. (2009). Analysis of Stokes flow in microchannels with superhydrophobic surfaces containing a periodic array of micro-grooves, *Microfluid. Nanofluid.* **7**(3): 353–382.

Teo, C. J. and Khoo, B. C. (2010). Flow past superhydrophobic surfaces containing longitudinal grooves: effects of interface curvature, *Microfluid. Nanofluid.* **9**(2-3): 499–511.

Wang, C.-Y. (1976). Parallel flow between corrugated plates, *ASCE J. Eng. Mech. Div.* **102**(6): 1088–1090.

Wang, C.-Y. (1979). On stokes flow between corrugated plates, *ASME J. Appl. Mech.* **46**(2): 462–464.

Wang, C.-Y. (1994). Flow in a channel with longitudinal ribs, *ASME J. Fluids Eng.* **116**(2): 233–237.

Wang, C.-Y. (1997). Stokes flow through a transversely finned channel, *ASME J. Fluids Eng.* **119**(1): 110–114.

Wang, C.-Y. (2003). Flow over a surface with parallel grooves, *Phys. Fluids* **15**(5): 1114–1121.

Wong, T.-S., Kang, S. H., Tang, S. K., Smythe, E. J., Hatton, B. D., Grinthal, A. and Aizenberg, J. (2011). Bioinspired self-repairing slippery surfaces with pressure-stable omniphobicity, *Nature* **477**(7365): 443–447.